

LEO-VL: Towards 3D Vision-Language Generalists via Data Scaling with Efficient Representation

Jiangyong Huang^{1,2} Xiaojian Ma² Xionghun Linghu² Yue Fan² Junchao He^{2,4} Wenxin Tan³
Qing Li² Song-Chun Zhu^{1,2,3} Yixin Chen² Baoxiong Jia² Siyuan Huang²

¹Peking University ²State Key Laboratory of General Artificial Intelligence, BIGAI

³Tsinghua University ⁴Beijing University of Posts and Telecommunications

<https://leo-vl.github.io>

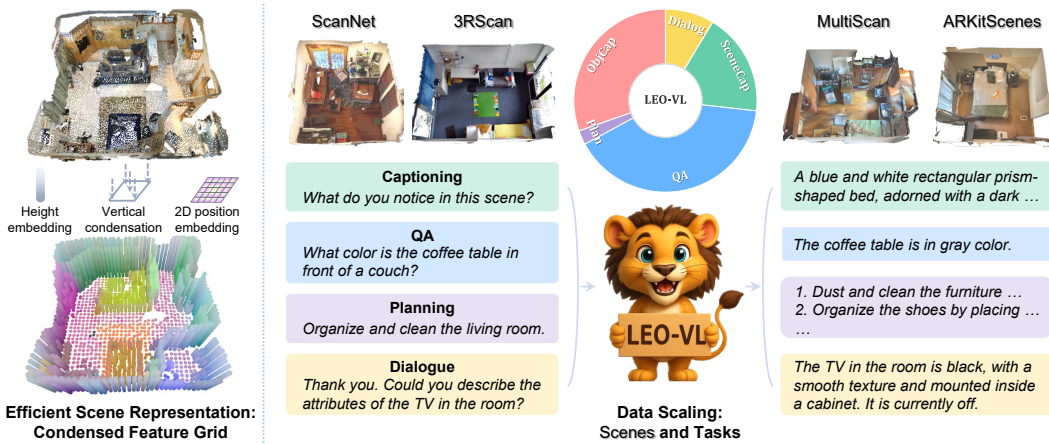


Figure 1: An overview of LEO-VL, a 3D vision-language (3D-VL) generalist. LEO-VL features an efficient scene representation with strong perception capability and low representation costs. We curate a comprehensive 3D-VL dataset across diverse scene domains and tasks for the instruction tuning of LEO-VL.

Abstract

Developing 3D-VL generalists capable of understanding 3D scenes and following natural language instructions to perform a wide range of tasks has been a long-standing goal in the 3D-VL community. Despite recent progress, 3D-VL models still lag behind their 2D counterparts in capability and robustness, falling short of the generalist standard. A key obstacle to developing 3D-VL generalists lies in data scalability, hindered by the lack of an efficient scene representation. We propose LEO-VL, a 3D-VL model built upon condensed feature grid (CFG), an efficient scene representation that bridges 2D perception and 3D spatial structure while significantly reducing token overhead. This efficiency unlocks large-scale training towards 3D-VL generalist, for which we curate over 700k high-quality 3D-VL data spanning four domains of real-world indoor scenes and five tasks such as captioning and dialogue. LEO-VL achieves state-of-the-art performance on a variety of 3D QA benchmarks, including SQA3D, MSQA, and Beacon3D. Ablation studies confirm the efficiency of our representation, the importance of task and scene diversity, and the validity of our data curation principle. Furthermore, we introduce SceneDPO, a novel post-training objective that enhances the robustness of 3D-VL models. We hope our findings contribute to the advancement of scalable and robust 3D-VL generalists.

1 Introduction

With the crucial role of 3D scene understanding in human intelligence, building generalist models that can understand 3D environments and communicate through natural language [34, 97, 78, 55] has become a central goal of the 3D vision-language (3D-VL) community. Recent progress has advanced capabilities across 3D-VL tasks such as grounding [117, 118, 39], captioning [53, 93], reasoning [32, 46], and dialogue [34, 95]. Nonetheless, current 3D-VL models fall significantly short of the generalist capabilities demonstrated by their 2D counterparts [60, 82, 88, 13, 42]. We posit that a key obstacle to developing 3D-VL generalists lies in data scalability, hindered by the absence of an efficient scene representation. Therefore, establishing an efficient and scalable scene representation is a critical first step towards building 3D-VL generalists.

Existing scene representations in 3D-VL models can be categorized into two approaches. The first adopts 3D modality inputs such as point clouds, but requires complex pre-processing pipelines such as 3D reconstruction and instance segmentation [117, 39, 11]. And they confront the inherent challenge of direct 3D perception, which is exacerbated by the scarcity of 3D-VL data. The other approach leverages 2D vision-language (2D-VL) models for perception [115, 111, 71], fueled by the advancement of 2D perception. However, this approach suffers from poor data scalability, as representing a 3D scene with multi-view 2D features incurs significant computational overhead. Additionally, both approaches typically use rudimentary 3D position embeddings for 3D spatial modeling, which fall short in capturing 3D spatial structures effectively.

We propose LEO-VL, a 3D-VL model built on condensed feature grid (CFG), an efficient scene representation that bridges 2D perception and 3D spatial structure, significantly improving efficiency while preserving the strength of 2D perception. Specifically, we employ a pretrained 2D visual encoder to extract image features, which are then back-projected into 3D space for voxelization. We utilize rotary position embedding (RoPE) [79] to encode the height of voxels and condense voxel features vertically to form a CFG. For horizontal spatial modeling, we integrate 2D Fourier features [80] into the CFG. In addition to efficiency, our CFG simplifies 3D spatial modeling by disentangling vertical and horizontal dimensions. The scene tokens of CFG are further connected to a large language model (LLM) for auto-regressive language modeling.

For the training of LEO-VL, we incorporate five 3D-VL tasks, including captioning, question answering (QA), planning, and dialogue, spanning four domains of real-world indoor scenes: ScanNet [19], 3RScan [86], MultiScan [58], and ARKitScenes [5]. Within each domain, we curate existing datasets and newly generated data while prioritizing data quality over scale. This could avoid model performance degradation from naive scaling with low-quality sources. With our curation principle, we collect a balanced and diverse corpus of over 700k high-quality 3D-VL data samples for the instruction tuning of LEO-VL.

We evaluate LEO-VL on a variety of 3D QA benchmarks, demonstrating state-of-the-art performance with significantly higher efficiency than prior methods. Ablation studies exhibit advantages of the CFG in efficiency and 3D spatial modeling. Ablations on various training data configurations reveal the benefits of tasks such as captioning and dialogue, and the importance of scene diversity for strong cross-domain performance. We further show that scaling with simplistic QA data leads to performance degradation, confirming our data curation principle, while our curated data yields consistent scaling effects. Additionally, we introduce SceneDPO, a novel post-training objective that incorporates contrasts across answers and scenes, and demonstrate its effectiveness in enhancing model robustness compared to conventional supervised finetuning (SFT).

In summary, our contributions are as follows:

1. We propose LEO-VL, a 3D-VL generalist built upon condensed feature grid (CFG), an efficient scene representation that enables strong capability in 3D scene perception with significantly improved efficiency and simplified 3D spatial modeling.
2. We construct a comprehensive 3D-VL instruction-tuning dataset spanning four scene domains and five tasks. Our dataset comprises over 700k high-quality samples, striking a balance between scale and quality, and serving as a reliable foundation for the training of 3D-VL generalists.
3. We demonstrate LEO-VL’s state-of-the-art performance across 3D QA benchmarks such as SQA3D. Ablation studies validate the efficiency of our representation, the benefits of task and domain diversity, and confirm our data curation principle. We also showcase the superiority of our post-training objective in enhancing model robustness compared to conventional SFT.

2 Related Work

3D Vision-Language Models. Early work in 3D-VL understanding develops models that process 3D representations such as point clouds [67, 69, 65, 45, 91, 68, 108, 37, 100] and voxels [27, 59, 74, 81, 28, 18, 15, 76]. With the maturation of pretraining and instruction tuning techniques, 3D-VL models have demonstrated significant performance improvements [109, 36, 1, 10, 36, 49, 94, 116, 117, 114, 90] and the capability of generalist models [29, 93, 34, 95, 11, 70, 118, 26, 107, 16, 32, 21]. Nonetheless, 3D perception remains challenging due to the data scarcity and inherent complexity of 3D representation space. In contrast, an alternative line of work leverages 2D perception models to handle 3D-VL tasks [64, 77, 23, 38, 31, 24, 57, 52], a strategy made increasingly effective by advances in 2D vision-language models (VLMs) [48, 88, 106, 115, 111, 71]. However, adapting 2D VLMs for 3D scene understanding poses two challenges: the cost of representing 3D scenes and the absence of effective 3D spatial modeling. While recent efforts [113, 99, 83, 33] attempt to address these issues, they still fall short of achieving both high efficiency and strong capability. In this work, we propose a framework that balances efficiency and effectiveness, showing the potential of foundational 3D-VL generalist models.

3D Vision-Language Datasets and Benchmarks. 3D-VL datasets and benchmarks are typically built upon 3D scene assets [19, 98, 86, 58, 5, 7, 73, 8, 41, 112, 25, 20]. Existing 3D-VL datasets primarily focus on object grounding [9, 2, 105] and QA [3, 56] tasks, but most of them are centered around ScanNet [19]. As the 3D-VL community advances, recent efforts have focused on aggregating diverse scene domains to enable large-scale pretraining [117, 118, 39, 89] and generalist instruction tuning [34]. This further drives the development of cross-domain datasets [96, 54, 46, 78, 102] and benchmarks [46, 35, 97]. Following this trend, our simple yet efficient framework is the first to scale 3D-VL generalist learning to the SceneVerse level [39], covering four scene domains [19, 86, 58, 5] and five 3D-VL tasks. We further demonstrate its effectiveness through comprehensive evaluations across these heterogeneous 3D scenes.

Vision-Language Learning Objective. Prior studies [22, 35, 63, 104] indicate that SFT, as a common learning objective for 3D-VL models, may undergo weak robustness given the scarce data and overfitting risk in 3D-VL learning. Existing efforts to remedy the robustness mainly involve data augmentation [96, 40, 110], with the learning objective underexplored. Motivated by the success of reinforcement learning from human feedback (RLHF) [61, 75, 72, 101, 62, 50, 17] for post-training, prior 2D-VL models [43, 66, 87, 92] employ direct preference optimization (DPO) objective [72] to address the robustness issue. We bring these insights into 3D-VL learning and introduce an additional objective with scene contrast to post-training for more robust 3D-VL models.

3 Method

In this section, we outline our approach to 3D-VL generalists. In Section 3.1, we introduce our model, LEO-VL, and particularly its efficient representation of 3D scenes, which largely reduces the token overhead while preserving strong perception capability. In Section 3.2, we introduce the recipe of our comprehensive instruction-tuning datasets for training of 3D-VL generalists. In Section 3.3, we further introduce a novel post-training objective to enhance the robustness of 3D-VL models.

3.1 Model

As illustrated in Fig. 2, LEO-VL extracts image features from RGBD frames and transforms the features into an efficient scene representation, termed the condensed feature grid (CFG). Next, an LLM performs auto-regressive language modeling over the joint sequence of CFG tokens and instruction tokens. In contrast to prior 3D-VL models that rely on object-centric 3D representation [34, 118, 32, 46], LEO-VL adopts 2D perception considering the limitations of the object-centric approach, such as the dependency of instance segmentation and loss of scene-level information.

2D Perception and Back-projection. We employ a 2D visual encoder to extract image features from multi-view RGB inputs. Given a set of RGB images $\{I_i \in \mathbb{R}^{H \times W \times 3}\}_{i=1}^N$, the encoder produces corresponding feature maps $\{m_i \in \mathbb{R}^{h \times w \times d}\}_{i=1}^N$, where h , w , and d denote the resolution and feature dimension. For each view, the corresponding depth maps $\{D_i \in \mathbb{R}^{H \times W}\}_{i=1}^N$ are used to back-project 2D pixels into 3D space. Let $K \in \mathbb{R}^{3 \times 3}$ and $T \in \mathbb{R}^{4 \times 4}$ denote the intrinsic and extrinsic camera

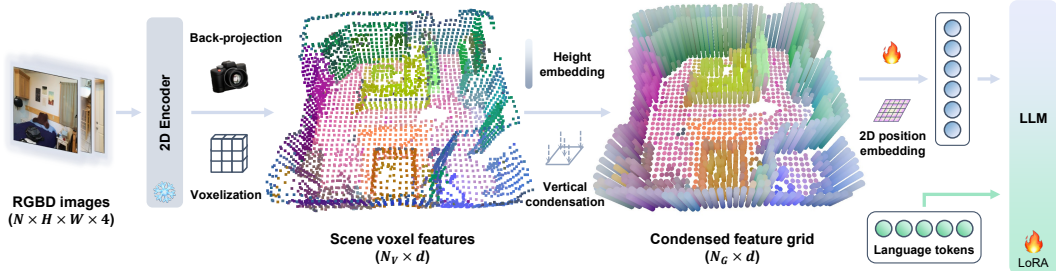


Figure 2: **Overview of LEO-VL model.** LEO-VL extracts 2D visual features from RGBD frames, and then transforms the features into CFG, significantly reducing the token overhead while preserving 3D spatial structure. An LLM performs auto-regressive language modeling based on the CFG tokens and instruction tokens.

matrices, respectively. A pixel at coordinate $q = (u, v)$ with depth $D(q)$ is back-projected to a 3D point (x, y, z) through the following homogeneous transformation:

$$\bar{p} = T \left[[D(q)K^{-1}\bar{q}]^T \parallel 1 \right]^T, \text{ where } \bar{p} = [x, y, z, 1]^T \text{ and } \bar{q} = [u, v, 1]^T.$$

We compute 3D coordinates for all pixels and interpolate them to align with the feature map resolution ($H \times W \rightarrow h \times w$). These 3D points are then associated with corresponding 2D features.

Condensed Feature Grid. First, we voxelize the 3D points and average pool the point features within each voxel, discarding empty voxels. For referring tasks such as object captioning, a learnable anchor embedding is injected into voxels that fall within the referred region. Despite voxelization, the representation remains costly and still limits scalability. To further improve efficiency, we convert voxels into the CFG by pooling voxel features along the height axis. Before pooling, we encode the height of each voxel with RoPE [79]. To encode horizontal positions, we integrate 2D Fourier features [80] in the CFG.

Position Embeddings. We adopt RoPE for vertical spatial modeling and Fourier features for horizontal spatial modeling. RoPE encodes position information by rotating the feature vector by a series of angles for different feature channels. The angles are derived from linear combinations of the position value and channel-specific frequencies. The rotary nature enables RoPE to better capture vertical spatial relations, such as distinguishing objects at different heights, compared to additive position embeddings [85, 80]. In contrast, the Fourier feature works by first applying a linear transformation to the position value and then computing sinusoidal components, which are passed through an MLP to produce embeddings. Let $R(p)$ denote the rotation matrix for RoPE and W the projection matrix for the Fourier feature. The formulations of position-encoded features are as follows:

$$f_{\text{RoPE}}(x, p) = R(p)x; \quad f_{\text{Fourier}}(x, p) = x + \text{MLP} \left(\left[\cos(2\pi Wp)^T \parallel \sin(2\pi Wp)^T \right]^T \right).$$

Large Language Model. The LLM takes as input the joint sequence of spatial-aware CFG tokens and language instruction tokens, and auto-regressively generates the response. We feed the LLM with scene tokens directly without any resampling process [118, 11] owing to the low token overhead.

3.2 Data

The construction of LEO-VL training data is guided by three principles: (1) the diversity in scene domains, which demonstrates crucial for 3D-VL learning [39]; (2) the diversity of tasks, which we think necessary given the benefits of long-response tasks [34, 54]; and (3) the balance between quality and scale, considering the potential risks in hindering model performance from low-quality data. We detail the composition of LEO-VL training data in Table 1.

Scene Domains. We include four domains of real-world indoor scenes: ScanNet [19], 3RScan [86], MultiScan [58], and ARKitScenes [5], following prior practices in scaling 3D scenes for 3D-VL learning [39, 46]. We exclude scene domains that lack attribute-rich scene graphs (*e.g.*, HM3D [73]), which are essential for LLM-assisted data generation. We follow the official splits for ScanNet and 3RScan, SceneVerse splits [39] for MultiScan, and MSQA splits [46] for ARKitScenes.

Table 1: **Overview of LEO-VL training data.** The entries include: “SV” for SceneVerse [39], “MM” for MMScan [54], ScanQA [3], “SQA” for SQA3D [56], MSQA [46], LEO [34], and “✓” for newly created data.

	ScanNet	3RScan	MultiScan	ARKitScenes	Overall count	Avg. length (str)	Avg. length (words)
ObjCap	SV, MM	LEO, SV, MM	SV	SV	216k	299	56
SceneCap	MM, ✓	LEO, MM, ✓	✓	✓	128k	633	104
QA	ScanQA, SQA, MSQA	MSQA	-	MSQA	289k	31	6
Plan	✓	LEO	✓	✓	18k	534	96
Dialog	✓	LEO	✓	✓	61k	93	18

Tasks and Datasets. We incorporate five prevalent 3D-VL tasks with natural language outputs, all compatible with a unified instruction tuning framework. We exclude the 3D object grounding task due to its different formulation. We think the absence of the grounding task is not detrimental given the success of 2D-VL generalists without explicit grounding supervision [47, 60, 88, 13]. In addition to existing datasets, we also generate new data by prompting LLMs with scene graphs [34, 46]. Our data covers five categories of text-output tasks:

- **Object Captioning.** This task requires the model to describe a specific object in natural language. We adopt object captions from SceneVerse [39] and MMScan [54]. We exclude datasets that repurpose object grounding texts as captions [14, 2], as such texts lack diverse descriptions regarding object attributes.
- **Scene Captioning.** This task requires generating comprehensive descriptions of entire 3D scenes. We use scene captions from LEO [34] and MMScan [54], and generate extra situated scene captions that incorporate situations to resolve spatial ambiguities (*e.g.*, left and right).
- **Question Answering.** In this task, the model answers general questions about the scene. We include ScanQA [3], SQA3D [56], and MSQA [46]. We avoid generating extra QA data, which we find tends to follow trivial patterns and may degrade model performance.
- **Planning.** Given a high-level goal (*e.g.*, “organize the room”), the model is required to generate a step-by-step grounded plan. We use the planning data from LEO [34] for 3RScan, and generate new data for other scene domains.
- **Dialogue.** This task requires the model to generate context-aware responses conditioned on both the 3D scene and dialogue history. We use the dialogue data from LEO [34] for 3RScan, and generate new data for other scene domains.

3.3 Post-training

Comprehensive instruction tuning alone may be insufficient to ensure model robustness, as evidenced by prior studies in 2D-VL models [43, 66, 87]. Given the pronounced risk of overfitting in 3D-VL models [22, 35], it is essential to design an effective post-training objective to enhance their robustness.

To this end, we propose ScenedPO, a novel learning objective for the post-training of 3D-VL models. First, we follow DPO to adopt a loss term \mathcal{L}_a that contrasts between positive answer a_\checkmark and negative answer a_\times . Motivated by the issue of visual ignorance [35] in 3D-VL models, where answers are predicted by overfitting to text without utilizing scene information, we introduce a loss term \mathcal{L}_s that contrasts between positive scene s_\checkmark and negative scene s_\times . This discourages model from predicting current answer when conditioned on irrelevant scenes. To mitigate degradation of positive answers, we also incorporate a negative log-likelihood loss term \mathcal{L}_{NLL} , which proves critical in prior works [50, 62, 87]. Given a training tuple $(s_\checkmark, s_\times, q, a_\checkmark, a_\times) \sim \mathcal{D}$, the overall loss \mathcal{L} is defined as follows:

$$\mathcal{L}_a = \mathbb{E}_{\mathcal{D}} \left[-\log \sigma \left(\beta_a \log \frac{\pi_\theta(a_\checkmark | s_\checkmark, q)}{\pi_{\text{ref}}(a_\checkmark | s_\checkmark, q)} - \beta_a \log \frac{\pi_\theta(a_\times | s_\checkmark, q)}{\pi_{\text{ref}}(a_\times | s_\checkmark, q)} \right) \right], \quad \mathcal{L}_{\text{NLL}} = \mathbb{E}_{\mathcal{D}} [-\log \pi_\theta(a_\checkmark | s_\checkmark, q)],$$

$$\mathcal{L}_s = \mathbb{E}_{\mathcal{D}} \left[-\log \sigma \left(\beta_s \log \frac{\pi_\theta(a_\checkmark | s_\checkmark, q)}{\pi_{\text{ref}}(a_\checkmark | s_\checkmark, q)} - \beta_s \log \frac{\pi_\theta(a_\checkmark | s_\times, q)}{\pi_{\text{ref}}(a_\checkmark | s_\times, q)} \right) \right], \quad \mathcal{L} = w_a \mathcal{L}_a + w_s \mathcal{L}_s + \mathcal{L}_{\text{NLL}},$$

where θ denotes the trained model, ref denotes the reference model, σ denotes the sigmoid function, and w_a, w_s, β_a , and β_s are scalar hyperparameters.

Table 2: **Comparison with state-of-the-art models on 3D-VL benchmarks.** Benchmarks are colorized according to scene domains: **ScanNet**, **3RScan**, and **ARKitScenes**. “C” stands for “CIDEr”, “B-4” for BLEU-4, “EM” for top-1 exact match, “EM-R” for refined top-1 exact match [34], and “Obj.” for object-centric metrics [35]. Gray figures indicate extra inductive bias in object order. † indicates the original results in the paper.

Model	Scene (#tokens)	ScanQA (val)		SQA3D (test)		MSQA (test)	Beacon3D		MSQA (test)	MSQA (test)
		C	B-4	EM	EM-R	GPT-Score	Case	Obj.	GPT-Score	GPT-Score
ScanQA [3]	Query (256)	64.9	10.1	47.2	-	-	-	-	-	-
3D-LLM [29]	Query (32)	74.5	12.9	49.8	-	-	-	-	-	-
PQ3D [118]	Query (80)	-	-	47.1	-	-	35.9	4.2	-	-
DSPNet [52]	Query (256)	-	-	50.4	-	-	-	-	-	-
3D-LLaVA [21]	Query (100)	92.6	17.1	54.5	56.6	-	-	-	-	-
3D-VisTA [117]	Object (80)	69.6	10.4	48.5	-	-	35.3†	8.1†	-	-
LEO [34]	Object (60)	101.4	13.2	50.0	52.4	56.7†	45.2	7.5	50.4†	59.7†
SceneVerse [39]	Object (80)	-	-	49.9	-	-	40.5	4.7	-	-
Chat-Scene [32]	Object (200)	87.7	14.3	54.6	57.5	-	45.8†	7.8†	-	-
Inst3D-LMM [99]	Object (200)	88.6	14.9	-	-	-	-	-	-	-
Scene-LLM [26]	Voxel (0.18m)	80.0	11.7	53.6	-	-	-	-	-	-
LLaVA-3D [115]	Voxel (3096)	91.7	14.5	55.6	57.6	-	-	-	-	-
Video-3D LLM [111]	Video (32 frames)	100.5	16.3	57.7	-	-	-	-	-	-
GPT4Scene [71]	Video (32 frames)	96.3	15.5	59.4	62.4	-	-	-	-	-
LEO-VL	Grid (750)	97.6	14.8	59.7	62.6	58.2	59.5	18.2	51.4	64.2

4 Experiment

In this section, we first compare LEO-VL against state-of-the-art models on a variety of 3D QA benchmarks in Section 4.1, highlighting its advantages in both efficiency and accuracy. In Section 4.2, we present ablation studies on model design to show the effectiveness of CFG. In Section 4.3, we analyze various training data configurations to reveal the influence of task diversity, scene domain coverage, data quality, and data scale on 3D-VL generalist learning. In Section 4.4, we further explore the effect of post-training objective based on LEO-VL.

Implementation Details. We initialize the 2D visual encoder and LLM with Qwen2.5-VL-7B-Instruct [4]. The learnable parameters include position embedding, anchor embedding, and LoRA parameters [30] of the LLM, which amount to 66M in total. We set the voxel size to 0.2 meters and retain up to 750 scene tokens of CFG. We train LEO-VL on our comprehensive 3D-VL dataset for 5 epochs, which takes 2 days with 8 NVIDIA A100 80G GPUs. We adopt AdamW optimizer [51] with a base learning rate at 3×10^{-5} , scheduled with linear warmup and cosine decay. We provide detailed hyperparameters in *Appendix*.

Evaluation. We primarily evaluate LEO-VL on 3D QA benchmarks considering the limited availability of standardized benchmarks for captioning, planning, and dialogue. Existing object captioning benchmarks [14, 2] are excluded in the main paper (see results in Table 8), as their captions are derived from object grounding texts with simplistic patterns that cannot reflect natural descriptive capabilities. Our evaluation includes ScanQA [3] for general QA in 3D scenes, SQA3D [56] for situated QA, and MSQA [46] for situated QA across multiple scene domains (*i.e.*, ScanNet, 3RScan, and ARKitScenes). We also incorporate Beacon3D [35], which offers robust metrics for 3D QA evaluation. Evaluation metrics include n-gram metrics (CIDEr and BLEU-4) for ScanQA, exact-match accuracy (EM and EM-R) for SQA3D, and GPT-Score for MSQA and Beacon3D.

4.1 Comparison with State-of-the-art Models

Baselines. For comparison, we include state-of-the-art 3D-VL models across four categories: (1) query-based methods, ranging from early work like ScanQA [3] to recent 3D-LLaVA [21]; (2) object-centric methods, from 3D-VisTA [117] to Inst3D-LMM [99]; (3) voxel-based methods, such as Scene-LLM [26] and LLaVA-3D [115]; and (4) video-based methods, including Video-3D LLM [111] and GPT4Scene [71]. We also report each model’s scene representation and its associated cost. For Scene-LLM, only the voxel size (0.18 meters) is available, which we estimate to yield a similar number of tokens as LLaVA-3D (voxel size 0.2 meters). For video-based methods, we list the number of frames, noting that 32 frames typically amount to over 6k scene tokens.

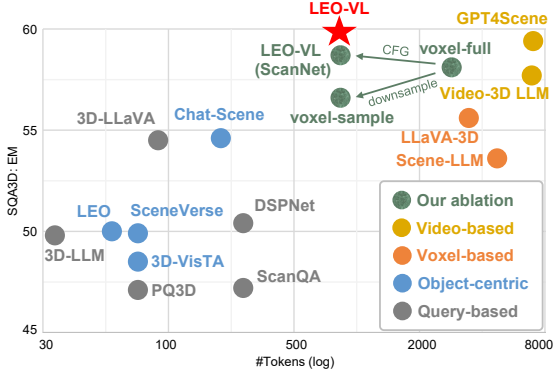


Figure 3: **Efficiency vs. accuracy on SQA3D.** LEO-VL reaches a Pareto optimum between efficiency and accuracy.

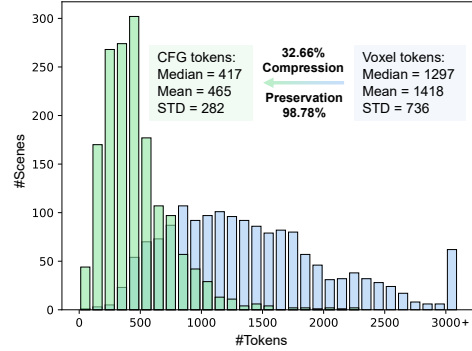


Figure 4: **Statistics of the CFG tokens and voxel tokens on ScanNet.**

Results. As shown in Table 2, LEO-VL achieves state-of-the-art performance on most 3D-VL benchmarks with a low representation cost. While video-based models show competitive performance, their representations involve thousands of tokens and limit data scalability, hindering the acquisition of generalist capabilities through large-scale training. In contrast, the efficient representation of LEO-VL enables 3D-VL data scaling for consistently strong performance across domains including ScanNet, 3RScan, and ARKitScenes. These results underscore the advantages of our efficient representation in perception capability and data scalability.

4.2 Model Analysis

Statistics. In Fig. 4, we present statistics of voxel tokens and CFG tokens on ScanNet. In addition to the distribution of token counts, we report two metrics: **compression rate**, defined as the ratio of CFG tokens to raw voxel tokens before condensation; and **preservation rate**, defined as the proportion of voxels retained by the CFG tokens. The results show that CFG achieves an average compression rate of about $\frac{1}{3}$ and an average preservation rate close to 99%. This demonstrates the high efficiency of our CFG representation.

Efficiency vs. Accuracy. We provide a joint visualization of efficiency and accuracy in Fig. 3. Accuracy is measured using the EM on SQA3D, the metric with the most available reference results. As shown in Fig. 3, LEO-VL achieves a Pareto optimum between efficiency and accuracy. To investigate the efficiency of CFG, we ablate the representation with two alternatives on the ScanNet subset: **voxel-full**, which retains all voxel tokens without condensation; and **voxel-sample**, which downsamples voxel tokens to match the token count of CFG. The results in Fig. 3 show that compared to voxel-full, voxel-sample suffers a drop in accuracy, while CFG even slightly improves the accuracy. These results suggest that high accuracy in 3D-VL tasks can be achieved with significantly lower token costs, as enabled by our efficient CFG representation.

3D Spatial Modeling. A key advantage of LEO-VL lies in the disentanglement of 3D spatial modeling across vertical and horizontal dimensions. To assess the effectiveness of position embeddings, we train LEO-VL on the ScanNet subset under two ablated settings: “**w/o z-pos**”, where the z-axis position embedding is removed; and “**w/o xyz-pos**”, where both z-axis and xy-plane position embeddings are removed. As shown in Fig. 5, both types of position embeddings play critical roles in 3D-VL tasks. Removing the z-axis position embedding leads to a general performance drop, while removing the xy-plane position embedding especially degrades performance on SQA3D. These results validate the effectiveness of our design in 3D spatial modeling.

4.3 Data Analysis

We conduct ablative studies on data to answer the following questions: (1) What is the effect of captioning, planning and dialogue tasks in 3D-VL generalist learning? (2) What is the benefit of scaling across diverse scene domains? (3) What happens when we naively scale up 3D-VL data without considering data quality? (4) How effective is data scaling for LEO-VL with curated data?

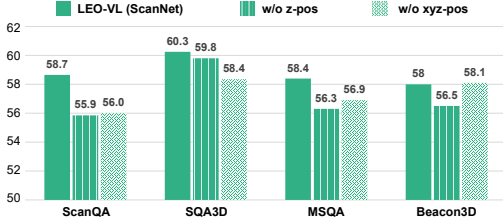


Figure 5: **Ablation on position embeddings.** This ablation study is conducted on the ScanNet subset. For more consistent visualization, we use the case-centric metric for Beacon3D, and averaged metrics for others.

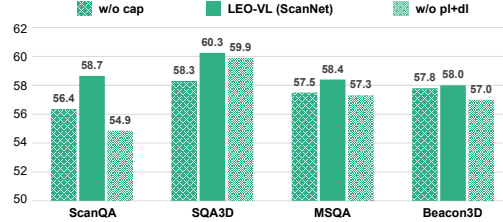


Figure 6: **Ablation on task effects.** This ablation study is conducted on the ScanNet subset. For more consistent visualization, we use the case-centric metric for Beacon3D, and averaged metrics for others.

Table 3: **Ablation results of scene domain scaling and simplistic QA data.** Benchmarks and metrics follow Table 2, with metrics averaged per benchmark.

Data	ScanQA	SQA3D	MSQA	Beacon3D	MSQA	MSQA	Avg.
ScanNet	58.7	60.3	58.4	37.9	46.1	54.7	52.7
Scan+3R	56.5	59.8	56.0	37.5	51.0	56.1	52.8
All	56.2	61.2	58.2	38.9	51.4	64.2	55.0
Scan+3R	56.5	59.8	56.0	37.5	51.0	56.1	52.8
+QA	55.7	58.3	56.8	37.5	51.3	55.6	52.5

Table 4: **QA Statistics.** “Extra QA” refers to additional simplistic QA data. “Top-15 coverage” denotes proportion of top-15 frequent answer templates.

	Count	Top-15 coverage
Scan+3R	253k	12.8%
Extra QA	669k	39.2%

Task Effects. Based on LEO-VL (ScanNet), we ablate the training data with different task configurations: “w/o cap” removes both object captioning and scene captioning tasks, while “w/o pl+dl” removes planning and dialogue tasks. As shown in Fig. 6, both task categories contribute meaningfully to the generalist capabilities of LEO-VL. Captioning proves particularly beneficial for SQA3D, whereas planning and dialogue tasks are more influential for ScanQA. We further perform a qualitative test by prompting “w/o cap” model with a scene captioning task. The model struggles to generate meaningful scene descriptions, likely due to the lack of training in captioning. These findings underscore the importance of task diversity for both acquiring task-specific skills and enhancing cross-task performance, thereby playing a critical role in achieving generalist capabilities.

Scene Domains. To assess the impact of scaling across scene domains, we introduce an additional checkpoint trained on ScanNet and 3RScan (Scan+3R), complementing existing LEO-VL and LEO-VL (ScanNet). As shown in Table 3, compared to “ScanNet”, “Scan+3R” yields significant improvements on 3RScan and ARKitScenes, with only a slight performance drop on ScanNet. Further, compared to “Scan+3R”, “All” shows substantial gains on ARKitScenes. These results suggest that the performance gains may primarily stem from exposure to corresponding domains, emphasizing the importance of a wide domain coverage for robust cross-domain generalist performances.

Priority of Quality over Scale. Based on the results of “Scan+3R”, we explore the outcome of naively scaling up 3D-VL data without considering data quality. Specifically, we augment our default subsets on ScanNet and 3RScan with extra 3D QA data from two sources: (1) LEO [34], which provides 94k QA samples from 3RScan; and (2) MMScan [54], which offers 575k QA samples from ScanNet and 3RScan. The resulting checkpoint is denoted as “+QA”. Notably, these two datasets exhibit a highly repetitive and simplistic answer distribution. To quantify this, we normalize the answers by replacing common entities with placeholders (*e.g.*, [COLOR]), transforming them into answer templates. As shown in Table 4, 39.2% of answers in “+QA” fall into the top-15 frequent templates, compared to only 12.8% in our curated data, demonstrating the simplistic distribution of “+QA”. The results in Table 3 reveal that despite incorporating substantially more QA data, “+QA” shows degradation in the overall performance compared to “Scan+3R”. This confirms that scaling with low-quality data can be detrimental, reinforcing our core curation principle: prioritizing data quality over sheer scale is essential for effective training of 3D-VL models.

Consistent Scaling Effects. To probe the scaling effects, we ablate the proportions of training data based on full-domain coverage, specifically training with 12.5%, 25%, 50%, and 100% of the dataset. We report the overall performance by averaging metrics across all evaluated benchmarks. As shown in Fig. 7, the results exhibit a steady upward trend, demonstrating consistent improvements as the data scale increases. This highlights a desirable scaling behavior enabled by our data design, echoing the noisy trend or even degradation in performance when scaling with low-quality 3D-VL data. The

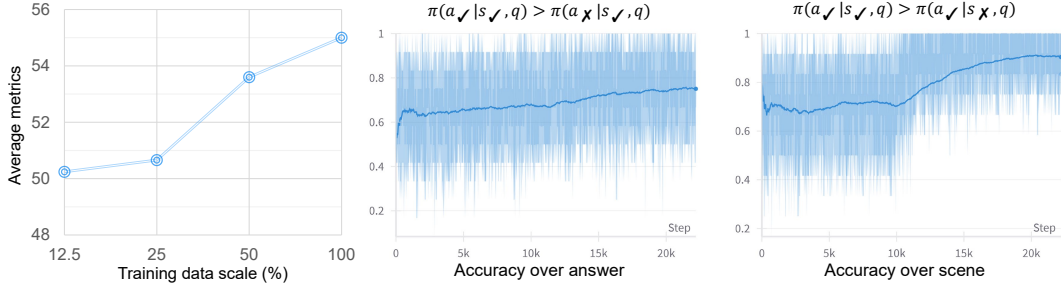


Figure 7: **LEO-VL scaling curve.** Figure 8: **Accuracy curves over answer and scene during post-training.**

consistent scaling effects underscore the importance of data curation in scaling for 3D-VL generalist training. Furthermore, the continued upward trend with no signs of saturation suggests that further performance gains may be achievable by scaling up more curated 3D-VL data.

4.4 Post-training

Settings. We explore the effect of post-training objective based on LEO-VL after instruction tuning. Specifically, we continue to fine-tune LEO-VL on SQA3D with SFT and SceneDPO, respectively. To construct negative answers a_{\times} , we first let LEO-VL generate predictions on the training set of SQA3D, and then employ GPT-4o [60] to rephrase correct predictions into hard negative samples. These rephrased negatives, along with the original incorrect predictions, form the negative answer set for SceneDPO. For negative scenes s_{\times} , we randomly sample a different scene from the training set. We evaluate the performance by two metrics: in-domain performance, computed as the average of EM and EM-R on SQA3D; and overall performance, averaged across all benchmarks. We remove the reference model in our implementation, given the empirical observation that it has a negligible impact while largely reducing resource costs. We set $w_a = 0.5$, $w_s = 0.5$, $\beta_a = 0.2$, $\beta_s = 0.03$, and train both SFT and SceneDPO for 10 epochs.

Results. The results are reported in Table 5 and Fig. 8. As shown in Table 5, SceneDPO improves both the in-domain performance on SQA3D and the overall performance across benchmarks, demonstrating its advantage in enhancing post-training performance. Fig. 8 shows consistent improvements in the accuracy over both answer and scene, indicating the acquisition of discriminative ability for the model. Notably, the significant gain in the accuracy over scene suggests the model’s evolution in addressing the issue of visual ignorance. On the other hand, the initially low accuracy also reveals the model’s limited ability in distinguishing semantically similar answers and correctly leveraging scene information for QA. This observation reinforces the need for effective post-training strategies like SceneDPO in enhancing the robustness of 3D-VL models.

Table 5: **Results of post-training on SQA3D.**

Data	SQA3D	Avg.
LEO-VL	61.2	55.0
SFT	62.5	53.7
SceneDPO	62.7	53.8

5 Conclusion

We propose LEO-VL, an advanced 3D-VL generalist that excels at general 3D-VL tasks with natural language outputs. LEO-VL is equipped with an efficient scene representation that bridges 2D perception and 3D spatial structure, featuring strong perception capability, high representation efficiency, and simplified 3D spatial modeling. For the generalist learning of LEO-VL, we curate a comprehensive 3D-VL dataset that spans four domains of real-world indoor scenes (*i.e.*, ScanNet, 3RScan, MultiScan, and ARKitScenes) and five tasks, covering captioning, QA, planning, and dialogue. We demonstrate the state-of-the-art performance of LEO-VL on various 3D QA benchmarks such as SQA3D. Ablative analyses reveal the importance of diversity in tasks and scene domains. The exploration with additional simplistic QA data confirms our principle that prioritizes data quality over scale, which naturally leads to consistent scaling effects. We hope our experience and findings in this work can benefit future research in developing 3D-VL generalists. Furthermore, we demonstrate the necessity and advantage of post-training objectives in enhancing the robustness of 3D-VL models.

References

- [1] Ahmed Abdelreheem, Ujjwal Upadhyay, Ivan Skorokhodov, Rawan Al Yahya, Jun Chen, and Mohamed Elhoseiny. 3dreftransformer: Fine-grained object identification in real-world scenes using natural language. In *Proceedings of Winter Conference on Applications of Computer Vision (WACV)*, 2022. 3
- [2] Panos Achlioptas, Ahmed Abdelreheem, Fei Xia, Mohamed Elhoseiny, and Leonidas Guibas. Referit3d: Neural listeners for fine-grained 3d object identification in real-world scenes. In *European Conference on Computer Vision (ECCV)*, 2020. 3, 5, 6
- [3] Daichi Azuma, Taiki Miyanishi, Shuhei Kurita, and Motoaki Kawanabe. Scanqa: 3d question answering for spatial scene understanding. In *Conference on Computer Vision and Pattern Recognition (CVPR)*, 2022. 3, 5, 6
- [4] Shuai Bai, Keqin Chen, Xuejing Liu, Jialin Wang, Wenbin Ge, Sibong Song, Kai Dang, Peng Wang, Shijie Wang, Jun Tang, et al. Qwen2.5-vl technical report. *arXiv preprint arXiv:2502.13923*, 2025. 6
- [5] Gilad Baruch, Zhuoyuan Chen, Afshin Dehghan, Tal Dimry, Yuri Feigin, Peter Fu, Thomas Gebauer, Brandon Joffe, Daniel Kurz, Arik Schwartz, et al. Arkitscenes: A diverse real-world dataset for 3d indoor scene understanding using mobile rgb-d data. *Advances in Neural Information Processing Systems Datasets and Benchmarks Track (NeurIPS Datasets and Benchmarks)*, 2021. 2, 3, 4
- [6] Daigang Cai, Lichen Zhao, Jing Zhang, Lu Sheng, and Dong Xu. 3djcq: A unified framework for joint dense captioning and visual grounding on 3d point clouds. In *Conference on Computer Vision and Pattern Recognition (CVPR)*, 2022. 18
- [7] Angel Chang, Angela Dai, Thomas Funkhouser, Maciej Halber, Matthias Niessner, Manolis Savva, Shuran Song, Andy Zeng, and Yinda Zhang. Matterport3d: Learning from rgb-d data in indoor environments. In *International Conference on 3D Vision (3DV)*, 2017. 3
- [8] Angel X Chang, Thomas Funkhouser, Leonidas Guibas, Pat Hanrahan, Qixing Huang, Zimo Li, Silvio Savarese, Manolis Savva, Shuran Song, Hao Su, et al. Shapenet: An information-rich 3d model repository. *arXiv preprint arXiv:1512.03012*, 2015. 3
- [9] Dave Zhenyu Chen, Angel X Chang, and Matthias Nießner. Scanrefer: 3d object localization in rgb-d scans using natural language. In *European Conference on Computer Vision (ECCV)*, 2020. 3, 17
- [10] Shizhe Chen, Pierre-Louis Guhur, Makarand Tapaswi, Cordelia Schmid, and Ivan Laptev. Language conditioned spatial relation reasoning for 3d object grounding. *Advances in Neural Information Processing Systems (NeurIPS)*, 2022. 3
- [11] Sijin Chen, Xin Chen, Chi Zhang, Mingsheng Li, Gang Yu, Hao Fei, Hongyuan Zhu, Jiayuan Fan, and Tao Chen. Ll3da: Visual interactive instruction tuning for omni-3d understanding, reasoning, and planning. In *Conference on Computer Vision and Pattern Recognition (CVPR)*, 2024. 2, 3, 4, 18
- [12] Sijin Chen, Hongyuan Zhu, Mingsheng Li, Xin Chen, Peng Guo, Yinjie Lei, Gang Yu, Taihao Li, and Tao Chen. Vote2cap-detr++: Decoupling localization and describing for end-to-end 3d dense captioning. *Transactions on Pattern Analysis and Machine Intelligence (TPAMI)*, 2024. 18
- [13] Zhe Chen, Jiannan Wu, Wenhai Wang, Weijie Su, Guo Chen, Sen Xing, Muyan Zhong, Qinglong Zhang, Xizhou Zhu, Lewei Lu, et al. Internvl: Scaling up vision foundation models and aligning for generic visual-linguistic tasks. In *Conference on Computer Vision and Pattern Recognition (CVPR)*, 2024. 2, 5
- [14] Zhenyu Chen, Ali Gholami, Matthias Nießner, and Angel X Chang. Scan2cap: Context-aware dense captioning in rgb-d scans. In *Conference on Computer Vision and Pattern Recognition (CVPR)*, 2021. 5, 6, 17, 18
- [15] Christopher Choy, JunYoung Gwak, and Silvio Savarese. 4d spatio-temporal convnets: Minkowski convolutional neural networks. In *Conference on Computer Vision and Pattern Recognition (CVPR)*, 2019. 3
- [16] Tao Chu, Pan Zhang, Xiaoyi Dong, Yuhang Zang, Qiong Liu, and Jiaqi Wang. Unified scene representation and reconstruction for 3d large language models. *arXiv preprint arXiv:2404.13044*, 2024. 3
- [17] Tianzhe Chu, Yuexiang Zhai, Jihan Yang, Shengbang Tong, Saining Xie, Dale Schuurmans, Quoc V Le, Sergey Levine, and Yi Ma. Sft memorizes, rl generalizes: A comparative study of foundation model post-training. In *International Conference on Machine Learning (ICML)*, 2025. 3

- [18] Angela Dai and Matthias Nießner. 3dmv: Joint 3d-multi-view prediction for 3d semantic scene segmentation. In *European Conference on Computer Vision (ECCV)*, 2018. 3
- [19] Angela Dai, Angel X Chang, Manolis Savva, Maciej Halber, Thomas Funkhouser, and Matthias Nießner. Scannet: Richly-annotated 3d reconstructions of indoor scenes. In *Conference on Computer Vision and Pattern Recognition (CVPR)*, 2017. 2, 3, 4
- [20] Matt Deitke, Eli VanderBilt, Alvaro Herrasti, Luca Weihs, Kiana Ehsani, Jordi Salvador, Winson Han, Eric Kolve, Aniruddha Kembhavi, and Roozbeh Mottaghi. Procthor: Large-scale embodied ai using procedural generation. *Advances in Neural Information Processing Systems (NeurIPS)*, 2022. 3
- [21] Jiajun Deng, Tianyu He, Li Jiang, Tianyu Wang, Feras Dayoub, and Ian Reid. 3d-llava: Towards generalist 3d llms with omni superpoint transformer. In *Conference on Computer Vision and Pattern Recognition (CVPR)*, 2025. 3, 6, 18
- [22] Weipeng Deng, Runyu Ding, Jihan Yang, Jiahui Liu, Yijiang Li, Xiaojuan Qi, and Edith Ngai. Can 3d vision-language models truly understand natural language? *arXiv preprint arXiv:2403.14760*, 2024. 3, 5
- [23] Runyu Ding, Jihan Yang, Chuhui Xue, Wenqing Zhang, Song Bai, and Xiaojuan Qi. Pla: Language-driven open-vocabulary 3d scene understanding. In *Conference on Computer Vision and Pattern Recognition (CVPR)*, 2023. 3
- [24] Mohamed El Banani, Amit Raj, Kevis-Kokitsi Maninis, Abhishek Kar, Yuanzhen Li, Michael Rubinstein, Deqing Sun, Leonidas Guibas, Justin Johnson, and Varun Jampani. Probing the 3d awareness of visual foundation models. In *Conference on Computer Vision and Pattern Recognition (CVPR)*, 2024. 3
- [25] Huan Fu, Bowen Cai, Lin Gao, Ling-Xiao Zhang, Jiaming Wang, Cao Li, Qixun Zeng, Chengyue Sun, Rongfei Jia, Binqiang Zhao, et al. 3d-front: 3d furnished rooms with layouts and semantics. In *International Conference on Computer Vision (ICCV)*, 2021. 3
- [26] Rao Fu, Jingyu Liu, Xilun Chen, Yixin Nie, and Wenhan Xiong. Scene-llm: Extending language model for 3d visual understanding and reasoning. In *Proceedings of Winter Conference on Applications of Computer Vision (WACV)*, 2025. 3, 6
- [27] Ben Graham. Sparse 3d convolutional neural networks. In *British Machine Vision Conference (BMVC)*, 2015. 3
- [28] Benjamin Graham, Martin Engelcke, and Laurens Van Der Maaten. 3d semantic segmentation with submanifold sparse convolutional networks. In *Conference on Computer Vision and Pattern Recognition (CVPR)*, 2018. 3
- [29] Yining Hong, Haoyu Zhen, Peihao Chen, Shuhong Zheng, Yilun Du, Zhenfang Chen, and Chuang Gan. 3d-llm: Injecting the 3d world into large language models. *Advances in Neural Information Processing Systems (NeurIPS)*, 2023. 3, 6
- [30] Edward J Hu, Yelong Shen, Phillip Wallis, Zeyuan Allen-Zhu, Yuanzhi Li, Shean Wang, Lu Wang, and Weizhu Chen. Lora: Low-rank adaptation of large language models. In *International Conference on Learning Representations (ICLR)*, 2022. 6, 17
- [31] Chenguang Huang, Oier Mees, Andy Zeng, and Wolfram Burgard. Visual language maps for robot navigation. In *International Conference on Robotics and Automation (ICRA)*, 2023. 3
- [32] Haifeng Huang, Yilun Chen, Zehan Wang, Rongjie Huang, Runsen Xu, Tai Wang, Luping Liu, Xize Cheng, Yang Zhao, Jiangmiao Pang, and Zhou Zhao. Chat-scene: Bridging 3d scene and large language models with object identifiers. *Advances in Neural Information Processing Systems (NeurIPS)*, 2024. 2, 3, 6, 18, 20
- [33] Hsiang-Wei Huang, Fu-Chen Chen, Wenhao Chai, Che-Chun Su, Lu Xia, Sanghun Jung, Cheng-Yen Yang, Jenq-Neng Hwang, Min Sun, and Cheng-Hao Kuo. Zero-shot 3d question answering via voxel-based dynamic token compression. In *Conference on Computer Vision and Pattern Recognition (CVPR)*, 2025. 3
- [34] Jianguo Huang, Silong Yong, Xiaojian Ma, Xiongkun Linghu, Puhao Li, Yan Wang, Qing Li, Song-Chun Zhu, Baoxiong Jia, and Siyuan Huang. An embodied generalist agent in 3d world. In *International Conference on Machine Learning (ICML)*, 2024. 2, 3, 4, 5, 6, 8, 17, 18, 20, 21
- [35] Jianguo Huang, Baoxiong Jia, Yan Wang, Ziyu Zhu, Xiongkun Linghu, Qing Li, Song-Chun Zhu, and Siyuan Huang. Unveiling the mist over 3d vision-language understanding: Object-centric evaluation with chain-of-analysis. In *Proceedings of the IEEE/CVF Conference on Computer Vision and Pattern Recognition (CVPR)*, 2025. 3, 5, 6, 18

- [36] Shijia Huang, Yilun Chen, Jiaya Jia, and Liwei Wang. Multi-view transformer for 3d visual grounding. In *Conference on Computer Vision and Pattern Recognition (CVPR)*, 2022. 3
- [37] Siyuan Huang, Yichen Xie, Song-Chun Zhu, and Yixin Zhu. Spatio-temporal self-supervised representation learning for 3d point clouds. In *International Conference on Computer Vision (ICCV)*, 2021. 3
- [38] Krishna Murthy Jatavallabhula, Alihusein Kuwajerwala, Qiao Gu, Mohd Omama, Tao Chen, Alaa Maalouf, Shuang Li, Ganesh Iyer, Soroush Saryazdi, Nikhil Keetha, et al. Conceptfusion: Open-set multimodal 3d mapping. In *Robotics: Science and Systems (RSS)*, 2023. 3
- [39] Baoxiong Jia, Yixin Chen, Huangyue Yu, Yan Wang, Xuesong Niu, Tengyu Liu, Qing Li, and Siyuan Huang. Sceneverse: Scaling 3d vision-language learning for grounded scene understanding. In *European Conference on Computer Vision (ECCV)*, 2024. 2, 3, 4, 5, 6, 20
- [40] Weitai Kang, Haifeng Huang, Yuzhang Shang, Mubarak Shah, and Yan Yan. Robin3d: Improving 3d large language model via robust instruction tuning. *arXiv preprint arXiv:2410.00255*, 2024. 3
- [41] Mukul Khanna, Yongsan Mao, Hanxiao Jiang, Sanjay Haresh, Brennan Shacklett, Dhruv Batra, Alexander Clegg, Eric Undersander, Angel X Chang, and Manolis Savva. Habitat synthetic scenes dataset (hssd-200): An analysis of 3d scene scale and realism tradeoffs for objectgoal navigation. In *Conference on Computer Vision and Pattern Recognition (CVPR)*, 2024. 3
- [42] Bo Li, Yuanhan Zhang, Dong Guo, Renrui Zhang, Feng Li, Hao Zhang, Kaichen Zhang, Peiyuan Zhang, Yanwei Li, Ziwei Liu, et al. Llava-onevision: Easy visual task transfer. *Transactions on Machine Learning Research (TMLR)*, 2024. 2
- [43] Shengzhi Li, Rongyu Lin, and Shichao Pei. Multi-modal preference alignment remedies regression of visual instruction tuning on language model. In *Annual Meeting of the Association for Computational Linguistics (ACL)*, 2024. 3, 5
- [44] Yang Li, Si Si, Gang Li, Cho-Jui Hsieh, and Samy Bengio. Learnable fourier features for multi-dimensional spatial positional encoding. *Advances in Neural Information Processing Systems (NeurIPS)*, 2021. 19
- [45] Yangyan Li, Rui Bu, Mingchao Sun, Wei Wu, Xinhan Di, and Baoquan Chen. Pointcnn: Convolution on x-transformed points. *Advances in Neural Information Processing Systems (NeurIPS)*, 2018. 3
- [46] Xiongkun Linghu, Jianguo Huang, Xuesong Niu, Xiaojian Ma, Baoxiong Jia, and Siyuan Huang. Multi-modal situated reasoning in 3d scenes. *Advances in Neural Information Processing Systems Datasets and Benchmarks Track (NeurIPS Datasets and Benchmarks)*, 2024. 2, 3, 4, 5, 6, 17, 18, 20
- [47] Haotian Liu, Chunyuan Li, Qingyang Wu, and Yong Jae Lee. Visual instruction tuning. *Advances in Neural Information Processing Systems (NeurIPS)*, 2023. 5
- [48] Haotian Liu, Chunyuan Li, Yuheng Li, and Yong Jae Lee. Improved baselines with visual instruction tuning. In *Conference on Computer Vision and Pattern Recognition (CVPR)*, 2024. 3
- [49] Minghua Liu, Ruoxi Shi, Kaiming Kuang, Yinhao Zhu, Xuanlin Li, Shizhong Han, Hong Cai, Fatih Porikli, and Hao Su. Openshape: Scaling up 3d shape representation towards open-world understanding. *Advances in Neural Information Processing Systems (NeurIPS)*, 2023. 3
- [50] Zhihan Liu, Miao Lu, Shenao Zhang, Boyi Liu, Hongyi Guo, Yingxiang Yang, Jose Blanchet, and Zhaoran Wang. Provably mitigating overoptimization in rlhf: Your sft loss is implicitly an adversarial regularizer. *Advances in Neural Information Processing Systems (NeurIPS)*, 2024. 3, 5
- [51] Ilya Loshchilov and Frank Hutter. Decoupled weight decay regularization. *arXiv preprint arXiv:1711.05101*, 2017. 6
- [52] Jingzhou Luo, Yang Liu, Weixing Chen, Zhen Li, Yaowei Wang, Guanbin Li, and Liang Lin. Dspnet: Dual-vision scene perception for robust 3d question answering. In *Conference on Computer Vision and Pattern Recognition (CVPR)*, 2025. 3, 6
- [53] Tiange Luo, Chris Rockwell, Honglak Lee, and Justin Johnson. Scalable 3d captioning with pretrained models. *Advances in Neural Information Processing Systems (NeurIPS)*, 2023. 2
- [54] Ruiyuan Lyu, Tai Wang, Jingli Lin, Shuai Yang, Xiaohan Mao, Yilun Chen, Runsen Xu, Haifeng Huang, Chenming Zhu, Dahua Lin, et al. Mmscan: A multi-modal 3d scene dataset with hierarchical grounded language annotations. *Advances in Neural Information Processing Systems Datasets and Benchmarks Track (NeurIPS Datasets and Benchmarks)*, 2024. 3, 4, 5, 8, 21

- [55] Xianzheng Ma, Yash Bhargat, Brandon Smart, Shuai Chen, Xinghui Li, Jian Ding, Jindong Gu, Dave Zhenyu Chen, Songyou Peng, Jia-Wang Bian, et al. When llms step into the 3d world: A survey and meta-analysis of 3d tasks via multi-modal large language models. *arXiv preprint arXiv:2405.10255*, 2024. 2
- [56] Xiaojian Ma, Silong Yong, Zilong Zheng, Qing Li, Yitao Liang, Song-Chun Zhu, and Siyuan Huang. Sqa3d: Situated question answering in 3d scenes. In *International Conference on Learning Representations (ICLR)*, 2023. 3, 5, 6
- [57] Yunze Man, Shuhong Zheng, Zhipeng Bao, Martial Hebert, Liang-Yan Gui, and Yu-Xiong Wang. Lexicon3d: Probing visual foundation models for complex 3d scene understanding. *Advances in Neural Information Processing Systems (NeurIPS)*, 2024. 3
- [58] Yongsen Mao, Yiming Zhang, Hanxiao Jiang, Angel Chang, and Manolis Savva. Multiscan: Scalable rgbd scanning for 3d environments with articulated objects. *Advances in Neural Information Processing Systems (NeurIPS)*, 2022. 2, 3, 4
- [59] Daniel Maturana and Sebastian Scherer. Voxnet: A 3d convolutional neural network for real-time object recognition. In *International Conference on Intelligent Robots and Systems (IROS)*, 2015. 3
- [60] OpenAI. Gpt-4 technical report. *arXiv preprint arXiv:2303.08774*, 2023. 2, 5, 9, 18, 20
- [61] Long Ouyang, Jeffrey Wu, Xu Jiang, Diogo Almeida, Carroll Wainwright, Pamela Mishkin, Chong Zhang, Sandhini Agarwal, Katarina Slama, Alex Ray, et al. Training language models to follow instructions with human feedback. *Advances in Neural Information Processing Systems (NeurIPS)*, 2022. 3
- [62] Richard Yuanzhe Pang, Weizhe Yuan, Kyunghyun Cho, He He, Sainbayar Sukhbaatar, and Jason Weston. Iterative reasoning preference optimization. *Advances in Neural Information Processing Systems (NeurIPS)*, 2024. 3, 5
- [63] Ruiying Peng, Kaiyuan Li, Weichen Zhang, Chen Gao, Xinlei Chen, and Yong Li. Understanding and evaluating hallucinations in 3d visual language models. *arXiv preprint arXiv:2502.15888*, 2025. 3
- [64] Songyou Peng, Kyle Genova, Chiyu Jiang, Andrea Tagliasacchi, Marc Pollefeys, Thomas Funkhouser, et al. Openscene: 3d scene understanding with open vocabularies. In *Conference on Computer Vision and Pattern Recognition (CVPR)*, 2023. 3
- [65] Anh Viet Phan, Minh Le Nguyen, Yen Lam Hoang Nguyen, and Lam Thu Bui. Dgcnn: A convolutional neural network over large-scale labeled graphs. *Neural Networks*, 2018. 3
- [66] Renjie Pi, Tianyang Han, Wei Xiong, Jipeng Zhang, Runtao Liu, Rui Pan, and Tong Zhang. Strengthening multimodal large language model with bootstrapped preference optimization. In *European Conference on Computer Vision (ECCV)*, 2024. 3, 5
- [67] Charles R Qi, Hao Su, Kaichun Mo, and Leonidas J Guibas. Pointnet: Deep learning on point sets for 3d classification and segmentation. In *Conference on Computer Vision and Pattern Recognition (CVPR)*, 2017. 3
- [68] Charles R Qi, Or Litany, Kaiming He, and Leonidas J Guibas. Deep hough voting for 3d object detection in point clouds. In *International Conference on Computer Vision (ICCV)*, 2019. 3
- [69] Charles Ruizhongtai Qi, Li Yi, Hao Su, and Leonidas J Guibas. Pointnet++: Deep hierarchical feature learning on point sets in a metric space. *Advances in Neural Information Processing Systems (NeurIPS)*, 2017. 3
- [70] Zhangyang Qi, Ye Fang, Zeyi Sun, Xiaoyang Wu, Tong Wu, Jiaqi Wang, Dahua Lin, and Hengshuang Zhao. Gpt4point: A unified framework for point-language understanding and generation. In *Conference on Computer Vision and Pattern Recognition (CVPR)*, 2024. 3
- [71] Zhangyang Qi, Zhixiong Zhang, Ye Fang, Jiaqi Wang, and Hengshuang Zhao. Gpt4scene: Understand 3d scenes from videos with vision-language models. *arXiv preprint arXiv:2501.01428*, 2025. 2, 3, 6, 18
- [72] Rafael Rafailov, Archit Sharma, Eric Mitchell, Christopher D Manning, Stefano Ermon, and Chelsea Finn. Direct preference optimization: Your language model is secretly a reward model. *Advances in Neural Information Processing Systems (NeurIPS)*, 2023. 3
- [73] Santhosh K Ramakrishnan, Aaron Gokaslan, Erik Wijmans, Oleksandr Maksymets, Alex Clegg, John Turner, Eric Undersander, Wojciech Galuba, Andrew Westbury, Angel X Chang, et al. Habitat-matterport 3d dataset (hm3d): 1000 large-scale 3d environments for embodied ai. *Advances in Neural Information Processing Systems Datasets and Benchmarks Track (NeurIPS Datasets and Benchmarks)*, 2021. 3, 4

- [74] Gernot Riegler, Ali Osman Ulusoy, and Andreas Geiger. Octnet: Learning deep 3d representations at high resolutions. In *Conference on Computer Vision and Pattern Recognition (CVPR)*, 2017. 3
- [75] John Schulman, Filip Wolski, Prafulla Dhariwal, Alec Radford, and Oleg Klimov. Proximal policy optimization algorithms. *arXiv preprint arXiv:1707.06347*, 2017. 3
- [76] Jonas Schult, Francis Engelmann, Alexander Hermans, Or Litany, Siyu Tang, and Bastian Leibe. Mask3d: Mask transformer for 3d semantic instance segmentation. In *International Conference on Robotics and Automation (ICRA)*, 2023. 3
- [77] Nur Muhammad Mahi Shafiullah, Chris Paxton, Lerrel Pinto, Soumith Chintala, and Arthur Szlam. Clip-fields: Weakly supervised semantic fields for robotic memory. In *Robotics: Science and Systems (RSS)*, 2023. 3
- [78] Chan Hee Song, Valts Blukis, Jonathan Tremblay, Stephen Tyree, Yu Su, and Stan Birchfield. Robospacial: Teaching spatial understanding to 2d and 3d vision-language models for robotics. In *Conference on Computer Vision and Pattern Recognition (CVPR)*, 2025. 2, 3
- [79] Jianlin Su, Murtadha Ahmed, Yu Lu, Shengfeng Pan, Wen Bo, and Yunfeng Liu. Roformer: Enhanced transformer with rotary position embedding. *Neurocomputing*, 2024. 2, 4, 18
- [80] Matthew Tancik, Pratul Srinivasan, Ben Mildenhall, Sara Fridovich-Keil, Nithin Raghavan, Utkarsh Singhal, Ravi Ramamoorthi, Jonathan Barron, and Ren Ng. Fourier features let networks learn high frequency functions in low dimensional domains. *Advances in Neural Information Processing Systems (NeurIPS)*, 2020. 2, 4, 19
- [81] Maxim Tatarchenko, Alexey Dosovitskiy, and Thomas Brox. Octree generating networks: Efficient convolutional architectures for high-resolution 3d outputs. In *International Conference on Computer Vision (ICCV)*, 2017. 3
- [82] Gemini Team, Rohan Anil, Sebastian Borgeaud, Jean-Baptiste Alayrac, Jiahui Yu, Radu Soricut, Johan Schalkwyk, Andrew M Dai, Anja Hauth, Katie Millican, et al. Gemini: a family of highly capable multimodal models. *arXiv preprint arXiv:2312.11805*, 2023. 2
- [83] Anh Thai, Songyou Peng, Kyle Genova, Leonidas Guibas, and Thomas Funkhouser. Splattalk: 3d vqa with gaussian splatting. *arXiv preprint arXiv:2503.06271*, 2025. 3, 18, 20
- [84] Hugo Touvron, Thibaut Lavril, Gautier Izacard, Xavier Martinet, Marie-Anne Lachaux, Timothée Lacroix, Baptiste Rozière, Naman Goyal, Eric Hambro, Faisal Azhar, et al. Llama: Open and efficient foundation language models. *arXiv preprint arXiv:2302.13971*, 2023. 18
- [85] Ashish Vaswani, Noam Shazeer, Niki Parmar, Jakob Uszkoreit, Llion Jones, Aidan N Gomez, Łukasz Kaiser, and Illia Polosukhin. Attention is all you need. *Advances in Neural Information Processing Systems (NeurIPS)*, 2017. 4, 18
- [86] Johanna Wald, Armen Avetisyan, Nassir Navab, Federico Tombari, and Matthias Nießner. Rio: 3d object instance re-localization in changing indoor environments. In *International Conference on Computer Vision (ICCV)*, 2019. 2, 3, 4
- [87] Fei Wang, Wenxuan Zhou, James Y Huang, Nan Xu, Sheng Zhang, Hoifung Poon, and Muhao Chen. mdpo: Conditional preference optimization for multimodal large language models. In *Annual Conference on Empirical Methods in Natural Language Processing (EMNLP)*, 2024. 3, 5
- [88] Peng Wang, Shuai Bai, Sinan Tan, Shijie Wang, Zhihao Fan, Jinze Bai, Keqin Chen, Xuejing Liu, Jialin Wang, Wenbin Ge, et al. Qwen2-vl: Enhancing vision-language model’s perception of the world at any resolution. *arXiv preprint arXiv:2409.12191*, 2024. 2, 3, 5
- [89] Tai Wang, Xiaohan Mao, Chenming Zhu, Runsen Xu, Ruiyuan Lyu, Peisen Li, Xiao Chen, Wenwei Zhang, Kai Chen, Tianfan Xue, et al. Embodiedscan: A holistic multi-modal 3d perception suite towards embodied ai. In *Conference on Computer Vision and Pattern Recognition (CVPR)*, 2024. 3
- [90] Yan Wang, Baoxiong Jia, Ziyu Zhu, and Siyuan Huang. Masked point-entity contrast for open-vocabulary 3d scene understanding. In *Conference on Computer Vision and Pattern Recognition (CVPR)*, 2025. 3
- [91] Wenxuan Wu, Zhongang Qi, and Li Fuxin. Pointconv: Deep convolutional networks on 3d point clouds. In *Conference on Computer Vision and Pattern Recognition (CVPR)*, 2019. 3
- [92] Yuxi Xie, Guanzhen Li, Xiao Xu, and Min-Yen Kan. V-dpo: Mitigating hallucination in large vision language models via vision-guided direct preference optimization. In *Findings of Annual Conference on Empirical Methods in Natural Language Processing (EMNLP Findings)*, 2024. 3

- [93] Runsen Xu, Xiaolong Wang, Tai Wang, Yilun Chen, Jiangmiao Pang, and Dahua Lin. Pointllm: Empowering large language models to understand point clouds. In *European Conference on Computer Vision (ECCV)*, 2024. 2, 3
- [94] Le Xue, Ning Yu, Shu Zhang, Artemis Panagopoulou, Junnan Li, Roberto Martín-Martín, Jiajun Wu, Caiming Xiong, Ran Xu, Juan Carlos Niebles, et al. Ulip-2: Towards scalable multimodal pre-training for 3d understanding. In *Conference on Computer Vision and Pattern Recognition (CVPR)*, 2024. 3
- [95] Jianing Yang, Xuweiyi Chen, Shengyi Qian, Nikhil Madaan, Madhavan Iyengar, David F Fouhey, and Joyce Chai. Llm-grounder: Open-vocabulary 3d visual grounding with large language model as an agent. In *International Conference on Robotics and Automation (ICRA)*, 2024. 2, 3
- [96] Jianing Yang, Xuweiyi Chen, Nikhil Madaan, Madhavan Iyengar, Shengyi Qian, David F Fouhey, and Joyce Chai. 3d-grand: A million-scale dataset for 3d-llms with better grounding and less hallucination. In *Conference on Computer Vision and Pattern Recognition (CVPR)*, 2025. 3
- [97] Jihan Yang, Shusheng Yang, Anjali W Gupta, Rilyn Han, Li Fei-Fei, and Saining Xie. Thinking in space: How multimodal large language models see, remember, and recall spaces. In *Conference on Computer Vision and Pattern Recognition (CVPR)*, 2025. 2, 3
- [98] Chandan Yeshwanth, Yueh-Cheng Liu, Matthias Nießner, and Angela Dai. Scannet++: A high-fidelity dataset of 3d indoor scenes. In *International Conference on Computer Vision (ICCV)*, 2023. 3
- [99] Hanxun Yu, Wentong Li, Song Wang, Junbo Chen, and Jianke Zhu. Inst3d-lmm: Instance-aware 3d scene understanding with multi-modal instruction tuning. In *Conference on Computer Vision and Pattern Recognition (CVPR)*, 2025. 3, 6
- [100] Xumin Yu, Lulu Tang, Yongming Rao, Tiejun Huang, Jie Zhou, and Jiwen Lu. Point-bert: Pre-training 3d point cloud transformers with masked point modeling. In *Conference on Computer Vision and Pattern Recognition (CVPR)*, 2022. 3
- [101] Weizhe Yuan, Richard Yuanzhe Pang, Kyunghyun Cho, Sainbayar Sukhbaatar, Jing Xu, and Jason Weston. Self-rewarding language models. In *International Conference on Machine Learning (ICML)*, 2024. 3
- [102] Jiahui Zhang, Yurui Chen, Yanpeng Zhou, Yueming Xu, Ze Huang, Jilin Mei, Junhui Chen, Yu-Jie Yuan, Xinyue Cai, Guowei Huang, et al. From flatland to space: Teaching vision-language models to perceive and reason in 3d. *arXiv preprint arXiv:2503.22976*, 2025. 3
- [103] Taolin Zhang, Sunan He, Tao Dai, Zhi Wang, Bin Chen, and Shu-Tao Xia. Vision-language pre-training with object contrastive learning for 3d scene understanding. In *AAAI Conference on Artificial Intelligence (AAAI)*, 2024. 18
- [104] Weichen Zhang, Ruiying Peng, Chen Gao, Jianjie Fang, Xin Zeng, Kaiyuan Li, Ziyou Wang, Jinqiang Cui, Xin Wang, Xinlei Chen, et al. The point, the vision and the text: Does point cloud boost spatial reasoning of large language models? *arXiv preprint arXiv:2504.04540*, 2025. 3
- [105] Yiming Zhang, ZeMing Gong, and Angel X Chang. Multi3drefer: Grounding text description to multiple 3d objects. In *International Conference on Computer Vision (ICCV)*, 2023. 3
- [106] Yuanhan Zhang, Jinming Wu, Wei Li, Bo Li, Zejun Ma, Ziwei Liu, and Chunyuan Li. Video instruction tuning with synthetic data. *arXiv preprint arXiv:2410.02713*, 2024. 3
- [107] Zhuofan Zhang, Ziyu Zhu, Pengxiang Li, Tengyu Liu, Xiaojian Ma, Yixin Chen, Baoxiong Jia, Siyuan Huang, and Qing Li. Task-oriented sequential grounding in 3d scenes. *arXiv preprint arXiv:2408.04034*, 2024. 3
- [108] Hengshuang Zhao, Li Jiang, Jiaya Jia, Philip HS Torr, and Vladlen Koltun. Point transformer. In *International Conference on Computer Vision (ICCV)*, 2021. 3
- [109] Lichen Zhao, Daigang Cai, Lu Sheng, and Dong Xu. 3dvg-transformer: Relation modeling for visual grounding on point clouds. In *International Conference on Computer Vision (ICCV)*, 2021. 3
- [110] Youjun Zhao, Jiaying Lin, Shuquan Ye, Qianshi Pang, and Rynson WH Lau. Openscan: A benchmark for generalized open-vocabulary 3d scene understanding. *arXiv preprint arXiv:2408.11030*, 2024. 3
- [111] Duo Zheng, Shijia Huang, and Liwei Wang. Video-3d llm: Learning position-aware video representation for 3d scene understanding. In *Conference on Computer Vision and Pattern Recognition (CVPR)*, 2025. 2, 3, 6, 18

- [112] Jia Zheng, Junfei Zhang, Jing Li, Rui Tang, Shenghua Gao, and Zihan Zhou. Structured3d: A large photo-realistic dataset for structured 3d modeling. In *European Conference on Computer Vision (ECCV)*, 2020. 3
- [113] Hongyan Zhi, Peihao Chen, Junyan Li, Shuailei Ma, Xinyu Sun, Tianhang Xiang, Yinjie Lei, Mingkui Tan, and Chuang Gan. Lscenellm: Enhancing large 3d scene understanding using adaptive visual preferences. In *Conference on Computer Vision and Pattern Recognition (CVPR)*, 2025. 3
- [114] Junsheng Zhou, Jinsheng Wang, Baorui Ma, Yu-Shen Liu, Tiejun Huang, and Xinlong Wang. Uni3d: Exploring unified 3d representation at scale. In *International Conference on Learning Representations (ICLR)*, 2024. 3
- [115] Chenming Zhu, Tai Wang, Wenwei Zhang, Jiangmiao Pang, and Xihui Liu. Llava-3d: A simple yet effective pathway to empowering llms with 3d-awareness. *arXiv preprint arXiv:2409.18125*, 2024. 2, 3, 6, 18
- [116] Haoyi Zhu, Honghui Yang, Xiaoyang Wu, Di Huang, Sha Zhang, Xianglong He, Hengshuang Zhao, Chunhua Shen, Yu Qiao, Tong He, et al. Ponderv2: Improved 3d representation with a universal pre-training paradigm. *Transactions on Pattern Analysis and Machine Intelligence (TPAMI)*, 2025. 3
- [117] Ziyu Zhu, Xiaojian Ma, Yixin Chen, Zhidong Deng, Siyuan Huang, and Qing Li. 3d-vista: Pre-trained transformer for 3d vision and text alignment. In *International Conference on Computer Vision (ICCV)*, 2023. 2, 3, 6, 18, 20
- [118] Ziyu Zhu, Zhuofan Zhang, Xiaojian Ma, Xuesong Niu, Yixin Chen, Baoxiong Jia, Zhidong Deng, Siyuan Huang, and Qing Li. Unifying 3d vision-language understanding via promptable queries. In *European Conference on Computer Vision (ECCV)*, 2024. 2, 3, 4, 6, 18, 20

A Discussion

Limitations. Despite strong performance and efficiency, LEO-VL exhibits several limitations. First, the use of the CFG effectively reduces token overhead but may lead to the loss of fine-grained details due to feature pooling, potentially limiting performance on tasks requiring precise understanding. Second, while the CFG’s effectiveness is demonstrated on indoor scenes, its generalization to outdoor or dynamic environments remains underexplored. Third, although our data scaling spans diverse real-world scene domains, the potential of leveraging abundant synthetic scenes is not explored yet.

Broader Impact. This work introduces a 3D-VL generalist model for 3D scene understanding tasks with natural language outputs, offering a step forward in enabling intelligent systems to comprehend and interact with the physical world. The proposed approach holds promise for applications such as assistive robotics, AR/VR interfaces, and digital twin systems for smart environments. Meanwhile, we recognize potential concerns related to data privacy, computational resource consumption, and misuse in surveillance. We encourage the community to pair technical innovation with ethical foresight. And we will release our code and data to support transparent, reproducible, and responsible research in 3D-VL generalists.

B Implementation Details

Input Sequence. Each input to the LLM begins with a system prompt, which is followed by the Scene Tokens, derived from the CFG, and then the Instruction, *i.e.*, the textual input. For situated tasks, the situation description is included within the Instruction, followed by task-specific text such as a question. The model then generates the Response, triggered by the generation prompt “assistant”.

```
<|im_start|>system
You are a helpful assistant.<|im_end|>
<|im_start|>user
<|vision_start|>{Scene Tokens}<|vision_end|>{Instruction}<|im_end|>
<|im_start|>assistant
{Response}
```

LLM Hyperparameters. We finetune the LLM using LoRA [30] for parameter-efficient learning, with a rank of 16, scaling factor $\alpha = 16$, and a dropout rate of 0, following LEO [34]. LoRA adapters are applied to all projection matrices: (W_q, W_k, W_v, W_o) in the attention layers and $(W_{gate}, W_{up}, W_{down})$ in the MLP blocks. For inference, we employ beam search with repetition and length penalties. Full hyperparameter settings are provided in Table 6.

Training Hyperparameters. We present the detailed settings in Table 7. The instruction tuning of LEO-VL is conducted for 5 epochs, and the post-training is conducted for 10 epochs.

GPT-Score. We calculate GPT-Score using the Azure OpenAI API with GPT-4o-2024-08-06 as the evaluator. Each score is evaluated based on a triplet consisting of a question, a ground-truth answer, and a predicted answer. We adopt the scoring prompt from MSR3D [46], which includes a system instruction and example contexts to guide the evaluation criteria.

C Additional Results

Scan2Cap. Scan2Cap [14] is a benchmark for 3D object captioning, which utilizes the referential text from ScanRefer [9] as captions. We have not included Scan2Cap results in the main paper as the captions are limited in linguistic diversity and offer limited insight into a model’s descriptive capability. Nonetheless, for completeness, we report the performance of LEO-VL finetuned on Scan2Cap in Table 8. The results show that LEO-VL achieves state-of-the-art performance on Scan2Cap, attaining the highest scores on two out of four evaluation metrics, highlighting its strong capability in object captioning.

ScanQA and SQA3D. We present extended results with more metrics for the experiments reported in the main paper. We report the full results for ScanQA in Table 9 and SQA3D in Table 10.

Table 6: Hyperparameters of the LLM.

Hyperparameter	Value
Training strategy	LoRA
Rank	16
Alpha	16
Dropout	0.0
Inference strategy	Beam search
Number of beams	5
Max new tokens	256
Repetition penalty	3.0
Length penalty	1.0

Table 7: Training hyperparameters of LEO-VL.

Hyperparameter	Value
Optimizer	AdamW
Weight decay	0.05
Betas	[0.9, 0.999]
Base learning rate	3×10^{-5}
Warmup steps	400
Type of GPUs	NVIDIA A100/A800 80G
Number of GPUs	8
Batch size per GPU (total)	2 (16)
Gradient accumulation steps	5
Training precision	bfloat16
Gradient norm	5.0

Table 8: Comparison with state-of-the-art models on Scan2Cap val set. We compare metrics under IoU@0.5.

Model	CIDEr	BLEU-4	METEOR	ROUGE
Scan2Cap [14]	35.2	22.4	21.4	43.5
3DJCG [6]	49.5	31.0	24.2	50.8
3D-VisTA [117]	66.9	34.0	27.1	54.3
Vote2Cap-DETR++ [12]	74.4	37.2	26.2	53.3
3DVLP [103]	54.4	34.1	34.3	54.3
LEO [34]	72.4	38.2	27.9	58.1
LL3DA [11]	65.2	36.8	26.0	55.1
PQ3D [118]	80.3	36.0	29.1	57.9
Chat-Scene [32]	77.2	36.3	28.0	58.1
LLaVA-3D [115]	79.2	41.1	30.2	63.4
3D-LLaVA [21]	78.8	36.9	27.1	57.7
Video-3D LLM [111]	80.0	40.2	28.5	61.7
GPT4Scene [71]	86.3	40.6	28.2	59.3
LEO-VL	77.3	43.8	30.3	64.9

MSQA. We extend the baseline coverage on the MSQA benchmark. Existing baselines for MSQA are relatively scarce, primarily because models generally require training on MSQA to attain reasonable performance, *i.e.*, zero-shot results tend to be poor. As only a handful of recent models have been trained on MSQA, the available baselines are limited. In Table 11, we report additional baselines and present more detailed metrics on the MSQA ScanNet subset, including GPT-4o [60], LEO [34], MSR3D [46], and SplatTalk [83]. Note that existing evaluation results on MSQA include two different versions of test data: the initially released version and a subsequent refined version. Results corresponding to the earlier version are marked with [†].

Beacon3D. Similar to MSQA, the Beacon3D benchmark also has evaluation results based on two versions of test data: an initial version corresponding to the results reported in the paper [35], and a refined version that is released. We denote results corresponding to the earlier version with [†]. In Table 12, we report the results on Beacon3D with more detailed metrics.

D Position Embedding

D.1 Rotary Position Embedding

Introduction. Position embeddings are essential in Transformer-based [85] architectures, which are inherently permutation-invariant. Traditional absolute position embeddings are simple but exhibit poor generalizability to longer sequences and limited capacity for capturing relative positions. RoPE [79] addresses these limitations by encoding positions as rotations in a complex plane. This formulation inherently supports relative position encoding and can generalize to sequences of unseen lengths. Due to these advantages, RoPE has been widely adopted in recent models such as LLaMA [84].

Table 9: Detailed results on ScanQA val set.

Model	CIDEr	BLEU-4	METEOR	ROUGE	EM	EM-R
<i>Domain scaling</i>						
LEO-VL (ScanNet)	101.1	16.2	19.6	47.4	23.0	45.9
LEO-VL (Scan+3R)	97.2	15.7	19.0	45.7	21.9	44.3
LEO-VL	97.6	14.8	19.2	46.1	22.2	45.0
<i>Voxel vs. CFG</i>						
voxel-full	101.5	15.7	20.0	48.0	23.3	46.4
voxel-sample	96.5	15.2	19.2	45.9	21.6	43.5
LEO-VL (ScanNet)	101.1	16.2	19.6	47.4	23.0	45.9
<i>Position embedding</i>						
w/o xyz-pos	97.7	14.3	19.2	46.1	21.9	44.2
w/o z-pos	97.1	14.6	19.1	46.1	21.8	44.0
LEO-VL (ScanNet)	101.1	16.2	19.6	47.4	23.0	45.9
<i>Task effects</i>						
w/o cap	97.9	14.8	19.2	46.2	22.3	44.3
w/o pl+dl	95.8	13.9	18.7	45.8	21.9	44.7
LEO-VL (ScanNet)	101.1	16.2	19.6	47.4	23.0	45.9
<i>Quality vs. scale</i>						
LEO-VL (Scan+3R)	97.2	15.7	19.0	45.7	21.9	44.3
+QA	96.4	14.9	18.9	45.4	22.0	43.1
<i>Data scaling</i>						
12.5%	79.2	10.6	15.9	39.6	19.4	38.3
25%	86.4	11.4	17.3	42.6	20.8	41.1
50%	94.8	13.6	18.7	44.7	21.2	42.0
LEO-VL	97.6	14.8	19.2	46.1	22.2	45.0
<i>Post-training on SQA3D</i>						
SFT	91.3	12.5	17.9	44.4	22.4	44.8
SceneDPO	92.8	13.1	18.4	45.1	22.7	44.4

Formulation. Let $x_p \in \mathbb{R}^d$ denote a feature vector at position p . RoPE decomposes x_p into a sequence of 2D subspaces and applies rotation matrices parameterized by channel-specific frequencies:

$$\text{RoPE}(x_p) = R_p x_p,$$

where the rotation matrix $R_p \in \mathbb{R}^{d \times d}$ is block-diagonal, composed of $\frac{d}{2}$ 2D rotation submatrices:

$$R_p = \begin{pmatrix} \cos p\theta_1 & -\sin p\theta_1 & 0 & 0 & \cdots & 0 & 0 \\ \sin p\theta_1 & \cos p\theta_1 & 0 & 0 & \cdots & 0 & 0 \\ 0 & 0 & \cos p\theta_2 & -\sin p\theta_2 & \cdots & 0 & 0 \\ 0 & 0 & \sin p\theta_2 & \cos p\theta_2 & \cdots & 0 & 0 \\ \vdots & \vdots & \vdots & \vdots & \ddots & \vdots & \vdots \\ 0 & 0 & 0 & 0 & \cdots & \cos p\theta_{\frac{d}{2}} & -\sin p\theta_{\frac{d}{2}} \\ 0 & 0 & 0 & 0 & \cdots & \sin p\theta_{\frac{d}{2}} & \cos p\theta_{\frac{d}{2}} \end{pmatrix},$$

with channel-specific frequencies $\theta_i = 10000^{-\frac{2i}{d}}$.

Height Encoding in 3D Scenes. We adopt RoPE to encode the voxel heights in 3D scenes considering its advantage in capturing height information during voxel feature pooling. As illustrated in Fig. 9, when two objects swap their heights, RoPE-encoded features can distinguish the configurations, whereas additive position embeddings fail. This property motivates our adoption of RoPE for the encoding of height information.

D.2 Fourier Features

Introduction. Fourier features [80, 44] focus on encoding multi-dimensional spatial positions, such as pixel positions in an image. Classical methods typically process each dimension independently and

Table 10: Detailed results on SQA3D test set.

Model	What	Is	How	Can	Which	Others	EM	EM-R
<i>Domain scaling</i>								
LEO-VL (ScanNet)	52.0	71.9	55.1	67.8	54.7	57.1	58.7	61.8
LEO-VL (Scan+3R)	50.2	71.8	54.0	69.2	57.8	56.5	58.3	61.3
LEO-VL	52.1	72.5	56.8	70.7	59.8	56.2	59.7	62.6
<i>Voxel vs. CFG</i>								
voxel-full	51.8	71.0	55.5	66.9	49.6	58.1	58.1	61.1
voxel-sample	49.0	69.8	51.4	68.0	55.8	54.6	56.6	59.7
LEO-VL (ScanNet)	52.0	71.9	55.1	67.8	54.7	57.1	58.7	61.8
<i>Position embedding</i>								
w/o xyz-pos	50.5	71.6	54.2	67.2	47.3	55.5	57.0	59.7
w/o z-pos	50.9	71.6	56.6	66.3	53.8	58.0	58.4	61.2
LEO-VL (ScanNet)	52.0	71.9	55.1	67.8	54.7	57.1	58.7	61.8
<i>Task effects</i>								
w/o cap	50.1	70.9	54.4	68.9	46.4	55.3	56.8	59.8
w/o pl+dl	52.7	71.9	53.5	68.9	53.0	55.3	58.4	61.4
LEO-VL (ScanNet)	52.0	71.9	55.1	67.8	54.7	57.1	58.7	61.8
<i>Quality vs. scale</i>								
LEO-VL (Scan+3R)	50.2	71.8	54.0	69.2	57.8	56.5	58.3	61.3
+QA	49.4	73.2	52.5	66.3	49.6	54.8	56.7	59.8
<i>Data scaling</i>								
12.5%	44.8	67.3	46.5	66.9	59.5	53.7	54.2	56.9
25%	46.4	67.3	48.6	64.8	53.3	55.1	54.4	57.1
50%	50.2	70.1	52.7	66.9	50.7	54.6	56.6	59.3
LEO-VL	52.1	72.5	56.8	70.7	59.8	56.2	59.7	62.6
<i>Post-training on SQA3D</i>								
SFT	53.0	73.3	55.5	68.3	65.2	60.8	61.0	64.0
SceneDPO	53.1	73.5	54.4	68.0	66.4	61.3	61.1	64.2

Table 11: Detailed results on MSQA (ScanNet) test set. * indicates text-only input, ‡ indicates zero-shot test, and † indicates evaluation results on the initial data version.

Model	Count.	Exist.	Attr.	Spatial	Navi.	Others	Overall
GPT-4o* [‡] [60]	32.3	79.3	79.0	37.0	31.7	91.6	52.3
LEO [34]	32.5	88.5	58.7	44.2	39.6	81.4	54.8
MSR3D [46]	32.3	93.1	50.0	46.5	54.1	75.6	54.2
SplatTalk ^{†‡} [83]	19.6	60.3	44.0	35.8	35.5	61.8	41.8
LEO-VL (ScanNet)	32.0	92.7	59.2	57.3	48.1	83.5	58.4
LEO-VL	36.3	93.8	59.2	56.0	44.6	83.5	58.2

Table 12: Detailed results on Beacon3D (ScanNet). † indicates evaluation results on the initial data version.

Model	Class	App.	Geo.	Spa.	Exi.	Overall (case)	Overall (obj.)
3D-VisTA [†] [117]	20.5	33.5	52.1	33.8	36.5	35.3	8.1
PQ3D [118]	37.8	45.8	32.1	19.2	44.5	35.9	4.2
SceneVerse [39]	26.4	40.4	40.0	35.0	54.1	40.5	4.7
LEO [34]	16.4	39.8	47.6	52.8	54.3	45.2	7.5
Chat-Scene [†] [32]	36.4	39.8	56.7	47.6	48.8	45.8	7.8
LEO-VL (ScanNet)	43.0	65.8	56.7	56.6	56.3	58.0	17.7
LEO-VL	43.0	68.6	57.8	57.2	58.0	59.5	18.2

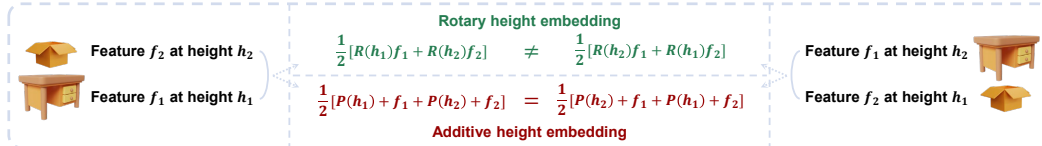


Figure 9: **Height encoding with RoPE.** When two objects swap their vertical positions, RoPE preserves the distinction in feature, while additive embeddings cannot.

then combine via concatenation. However, this falls short in capturing holistic spatial relations such as Euclidean distances, and struggles with generalizing to unbounded ranges of multi-dimensional coordinates. Fourier features overcome these issues by mapping the low-dimensional coordinates into a high-dimensional periodic function space, enabling better modeling of multi-dimensional positions.

Formulation. Given an n -dim spatial coordinate $p \in \mathbb{R}^n$ and a projection matrix $W \in \mathbb{R}^{\frac{d}{2} \times n}$ (where d is the feature dimension), the Fourier feature $F \in \mathbb{R}^d$ is computed as:

$$F = [\cos(2\pi Wp)^T \parallel \sin(2\pi Wp)^T]^T,$$

where $W \sim \mathcal{N}(0, 1)$ is initialized from a Gaussian distribution. The resulting feature vector is then scaled by $\frac{1}{\sqrt{d}}$ for normalization and passed through an MLP to generate the final position embedding, which is subsequently added to the original feature vector x_p .

E Data Statistics

Additional Simplistic QA Data. In the main paper, we explore the outcome of naively scaling with low-quality 3D-VL data. The additional QA data is sourced from LEO [34] (94k from 3RScan) and MMScan [54] (575k from ScanNet and 3RScan). This part of data exhibits a simplistic distribution with limited answer diversity. By categorizing answers into placeholder-based templates, we observe a significantly higher proportion of the top-15 frequent answer templates in the additional QA data (39.2% vs. 12.8%). The templates and their distribution are visualized in Figs. 10 and 11.

F Qualitative Examples

We present qualitative results of LEO-VL performing various tasks in Fig. 12.

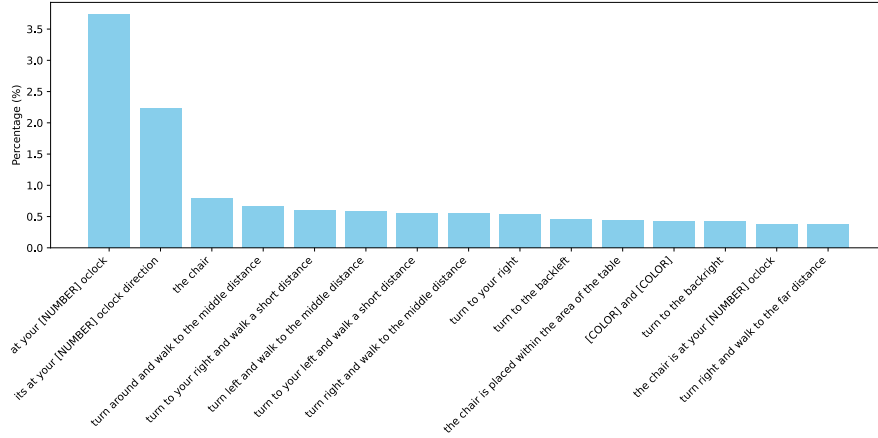


Figure 10: Top-15 frequent answer templates (12.8%) in our default QA data on ScanNet and 3RScan.

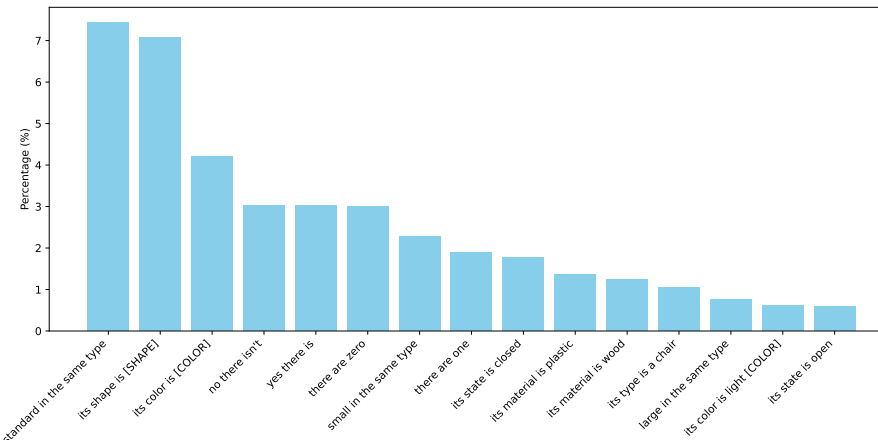


Figure 11: Top-15 frequent answer templates (39.2%) in the additional QA data on ScanNet and 3RScan.

	<p>Instruction: Detail the object at the selected spot.</p> <p>Response: The nightstand is a wooden furniture piece with a rectangular shape and a brown color. It has two drawers and a shelf, and can be used as a bedside table. The texture of the nightstand is wooden, and it has a simple and classic design.</p>		<p>Instruction: I am inspecting the trash can. Draft a concise portrayal of this 3D scene.</p> <p>Response: To my left, in the middle distance, there is a black and silver stove. It's made of metal and glass, used for cooking with a smooth and glossy texture. The stove has a flat top with burners and a control panel, and it's currently off. In the middle distance to my right, there is a kitchen cabinet. This room appears to be a well-equipped kitchen or dining area, with various appliances, storage solutions, and seating options.</p>
	<p>Instruction: Look at the organizer shelf next to the desk, is it taller or shorter than the desk?</p> <p>Response: Taller.</p>		<p>Instruction: Provide a directive for the task: organize and tidy up the living area.</p> <p>Response: 1. Dust and clean the surfaces of the furniture, such as the sofa, table, and cabinet. 2. Organize items on the table, ensuring that they are neatly arranged and not cluttered. 3. Clean the TV screen and ensure it is turned off when not in use. 4. Sweep or vacuum the floor to remove any dirt or debris. 5. Adjust the position of the sofa if needed for better seating arrangement. 6. Check and adjust the temperature of the heater if necessary. 7. Remove any unnecessary items or clutter from the living area to create a more organized space.</p>
	<p>Instruction: Can you tell me the location of the remote control?</p> <p>Response: The remote control is placed within the area of the TV stand.</p> <p>Instruction: Where can I find the monitor in the room?</p> <p>Response: The monitor is resting on the desk.</p> <p>Instruction: Thanks for the detailed information.</p> <p>Response: You're welcome! If you have any more questions, feel free to ask.</p>		

Figure 12: Qualitative results of LEO-VL on various tasks. The left column shows object captioning, QA, and dialogue; the right column shows scene captioning and planning.